Article

A Microtopographic Feature Analysis-Based LiDAR Data Processing Approach for the Identification of Chu Tombs

Shaohua Wang [1], Qingwu Hu [2,3,*] iD, Fengzhu Wang [4], Mingyao Ai [3] and Ruofei Zhong [2]

[1] School of International Software, Wuhan University, No. 129, Luoyu Road, Wuhan 430079, China; shwang@whu.edu.cn

[2] Beijing Advanced Innovation Center for Imaging Technology, Capital Normal University, Beijing 100048, China; zrf@cnu.edu.cn

[3] School of Remote Sensing and Information Engineering, Wuhan University, No. 129, Luoyu Road, Wuhan 430079, China; aimingyao@whu.edu.cn

[4] Cultural Heritage Bureau of Hubei Province, Gongzheng Road, Wuhan 430071, China; fengzhuwang@163.com

* Correspondence: huqw@whu.edu.cn; Tel.: +86-189-710-70362

Abstract: Most of the cultural sites hidden under dense vegetation in the mountains of China have been destroyed. In this paper, we present a microtopographic feature analysis (MFA)-based Light Detection and Ranging (LiDAR) data processing approach and an archaeological pattern-oriented point cloud segmentation (APoPCS) algorithm that we developed for the classification of archaeological objects and terrain points and the detection of archaeological remains. The archaeological features and patterns are interpreted and extracted from LiDAR point cloud data to construct an archaeological object pattern database. A microtopographic factor is calculated based on the archaeological object patterns, and this factor converts the massive point cloud data into a raster feature image. A fuzzy clustering algorithm based on the archaeological object patterns is presented for raster feature image segmentation and the detection of archaeological remains. Using the proposed approach, we investigated four typical areas with different types of Chu tombs in Central China, which had dense vegetation and high population densities. Our research results show that the proposed LiDAR data processing approach can identify archaeological remains from large-volume and massive LiDAR data, as well as in areas with dense vegetation and trees. The studies of different archaeological object patterns are important for improving the robustness of the proposed APoPCS algorithm for the extraction of archaeological remains.

Keywords: archaeological object; LiDAR; Microtopographic feature analysis; fuzzy cluster; feature extraction

1. Introduction

Advances in remote sensing and space-based imaging have led to an increased understanding of settlements and landscapes from space and their spatial layouts. During the past 50 years, aerial photos and satellite images have been the most common remote sensing data sources used in the field of archaeological identification, investigation, and surveying [1–3]. Visible spectral, infrared, and multispectral remote sensing are the most common remote sensing approaches, and have been used extensively to identify targets linked to the presence of archaeological earthworks and remains [3–8].

Dense vegetation and trees pose considerable challenges during the identification of archaeological remains hidden in vegetation, especially in regions south of 30° latitude.

Airborne laser scanning (ALS) using Light Detection and Ranging (LiDAR) technology provides a highly detailed three-dimensional record of the ground as seen from the air by the reflection of a scanning laser beam. This method has revolutionized the field of topographic surveying [9,10]. The laser beam can penetrate vegetation to accurately obtain terrain characteristics in areas of dense vegetation and reveal extant archaeological earthwork features. This approach has proven its utility in remote sensing-based archaeological investigations and landscape studies in forested and non-forested areas [5,11–26].

LiDAR data processing and its application to archaeological identification, investigation, and surveying are based on point cloud filtering and classification, which are performed to extract the microtopographic relief of archaeological features [27–29]. Recent studies on the use of LiDAR in archaeological studies have achieved considerable progress, especially in the investigation and identification of archaeological earthworks and remains, even in forested areas with dense vegetation. However, the use of LiDAR in archaeology still faces serious challenges. Notably, archaeological earthworks and remains have different geometry features and patterns than the terrain; thus, the current LiDAR data processing technologies for traditional terrain surveying and modeling are not suitable for archaeological object extraction and classification. Developing a LiDAR data processing approach to extract archaeological information from raw LiDAR point cloud data remains a challenging and valuable research area. The current LiDAR point cloud filtering and classification approach is designed for terrain surveying and mapping to generate a digital elevation model (DEM) [30–32]. In DEM generation, the ground structures of artificial works should be removed via special topographic calculations that treat archaeological remains as artificial structures. Another major challenge is that the feature extraction algorithms of point cloud data are related to specific archaeological remains. Additionally, the LiDAR processing approaches for ancient walls, buildings and tombs are quite different, and these differences limit the application of LiDAR in remote sensing-based archaeology [33–35].

In this paper, we present a microtopographic feature analysis (MFA)-based LiDAR data processing approach and an archaeological pattern-oriented point cloud segment (APoPCS) algorithm that we designed for the classification of archaeological objects and terrain points for the detection of archaeological remains. The archaeological features and patterns are interpreted and extracted from the LiDAR point cloud to build an archaeological object pattern database. A microtopographic factor is calculated based on the archaeological object pattern using LiDAR point cloud data, which are converted to a raster feature image. A fuzzy cluster algorithm that considers archaeological object patterns is presented to segment the raster feature image and detect archaeological remains. Using the proposed approach for archaeological remains extraction, we selected four typical areas with different types of Chu tombs, dense vegetation, and large populations in Central China. Our research results show that the proposed LiDAR data processing approach can identify and extract the archaeological remains from large-volume and massive LiDAR data, as well as in areas with dense vegetation and trees. The study of different archaeological object patterns is important to the proposed APoPCS algorithm for the robust extraction of archaeological remains.

2. Background

2.1. The Study Area: Balingshan Chu Tomb Group in Jingzhou, China

The study area (33°20′–33°30′N, 112°00′–112°10′E) is located approximately 17 km northwest of Yingcheng, the first Chu Imperial City, which was built in B.C. 689 (Figure 1). Yingcheng and Balingshan are located in different parts of the Jing Mountains. In the southeast corner of this region, the Yingcheng Relic Site was excavated in 1965. Yingcheng was the Imperial City for more than four hundred years before the Qing Dynasty turned it into ruins in B.C. 278. The Zhujiatai site, a new Stone Age relic, is also located in this region. The Balingshan district is an important area for tomb research.

Notably, the tombs of 30 empires were noted in the historical documents and records, and most of them are Chu tombs [36,37]. These Chu tombs are numerous, totaling approximately 300, and vary in type. They include empire tombs, nobility tombs, civilian tombs, and slave tombs, and this diversity is extremely useful and important for studying the hierarchy of the Chu Empire.
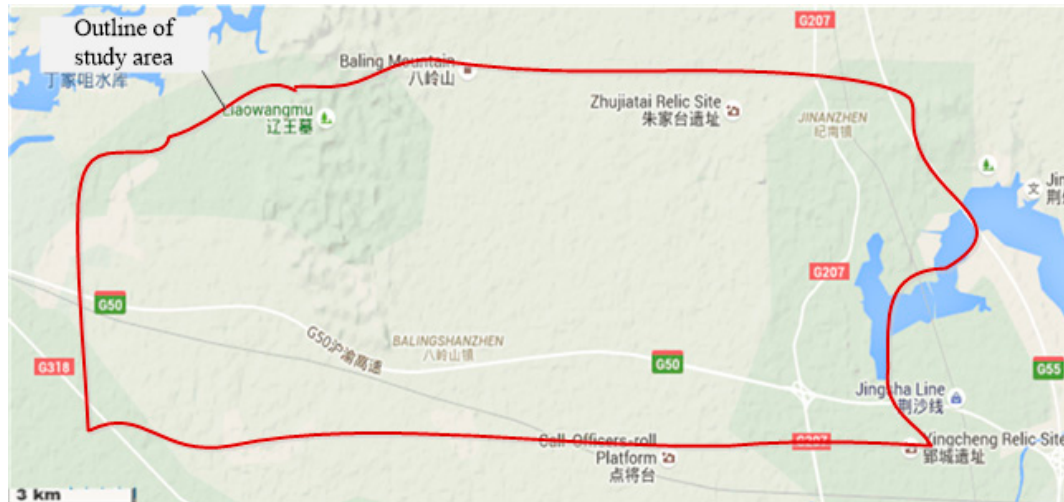

Figure 1. Study Area: Balingshan Chu Tomb Group.

2.2. Difficulties of Tomb Investigation in Balingshan

As the documented research suggests, the Balingshan district is a historical and traditional tomb area. There are many tombs in this area, including those of 18 Chu kings, kings from other empires, many nobles, and countless residents. Locating the Chu tombs via remote sensing-based archaeology is a major challenge in Balingshan. Specifically, three main difficulties exist for Chu tomb investigation in Balingshan:

(1) The Balingshan district is located at the intersection of the Yangtze River and the Hanjiang River. Plenty of rain and a suitable climate cause Balingshan to be fully covered by vegetation (Figure 2). The average height of trees is above 8 m. Thus, LiDAR should be used to overcome the traditional limitation of dense vegetation cover and identify archaeological remains.

Figure 2. Tombs under dense vegetation.

(2) There are many tombs from different years in the Balingshan district. Our research focuses on the Chu tombs, which are more than 2000 years old and urgently need to be protected. Both human activities and natural vicissitude have gradually damaged the Chu tombs, potentially ruining the bodies. Information about the ruins is scarce, and only some of the Chu tombs exist at the Earth's surface. It is difficult to identify the Chu tombs from the ground, and a section of the Chu tombs were

submerged under the terrain. The traditional LiDAR filtering and classification approach will interpret the sporadic distribution of the tombs in the study area as normal artificial objects and then remove them. Thus, creating a LiDAR data processing approach to extract the Chu tombs is a major challenge based on traditional LiDAR filtering and classification methods.

(3) The Balingshan district is located near the economic center of Jingzhou City. This district also has many residential blocks and a dense road network that may partly change the state of archaeological remains (Figure 3). The Chu tomb identification approach should combine all the existing ruin information and use spatial analysis and computations to obtain full descriptions of the Chu tombs.
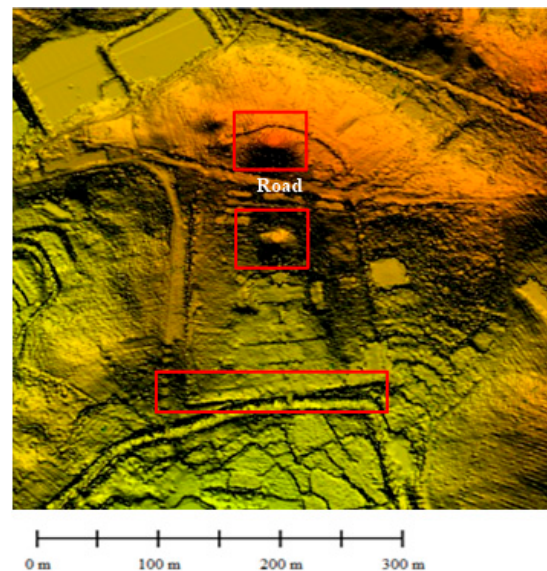

Figure 3. Tomb divided by a road network and residential blocks.

3. Methodology

3.1. Framework of the Proposed Approach

The proposed Chu tomb identification approach based on LiDAR data involves a special segment-by-segment LiDAR processing and analysis approach for the extraction and identification of archaeological remains that are hidden below the Earth's surface. The proposed approach is divided into five parts: LiDAR data collection, the filtering and classification of ground points, pattern analysis of Chu tombs in the point cloud, feature transformation and extraction, and verification with visible remote sensing. The detailed framework of the technique is shown in Figure 4.

As Figure 4 shows, airborne laser scanning (ALS) is used to obtain LiDAR data in the study area, including point cloud data and visible raster images. The point density is very important in studies of archaeological remains. An adequate point density can ensure that the detailed information of partial tomb segments is preserved, while a high point density requires more routes and a low airline height, which is associated with low efficiency and high costs. The determination of LiDAR point density is based on the geometric features of specific archaeological remains in different decades. In this paper, the density of the point cloud was no less than 16 pts/m^2, considering the Chu tombs are from 2000 years ago. A Trimble Harrier 56 ALS [38,39] was adopted for data collection with a Y-12 airplane. The normal flight height of a Y-12 should be above 500 m, which can only obtain approximately 10 pts/m^2 with the Harrier 56 ALS. To obtain a point cloud with more than 16 pts/m^2, a grid is designed to collect the laser scanning data, as shown Figure 5. Normally, east–west horizontal lines are adopted in most LiDAR datasets (shown as black lines in Figure 5). The additional north–south vertical lines are added to increase the density of LiDAR points. The two datasets are matched by direct georeferencing in WGS 84 coordinates, which are recorded by the ALS.
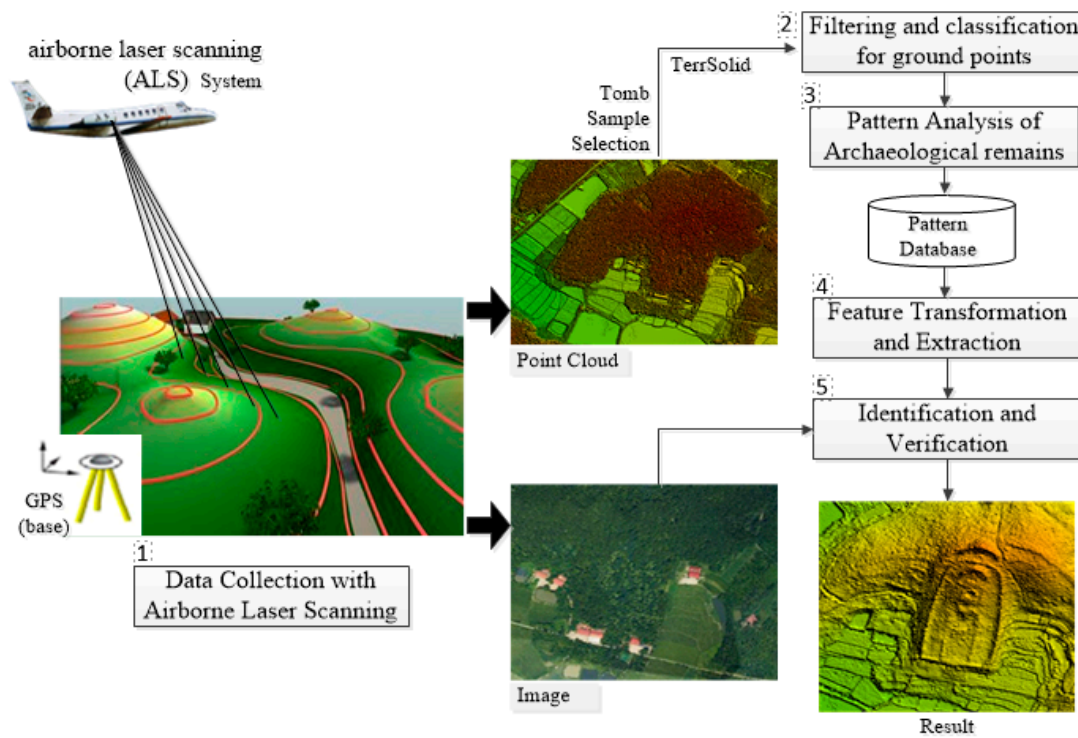
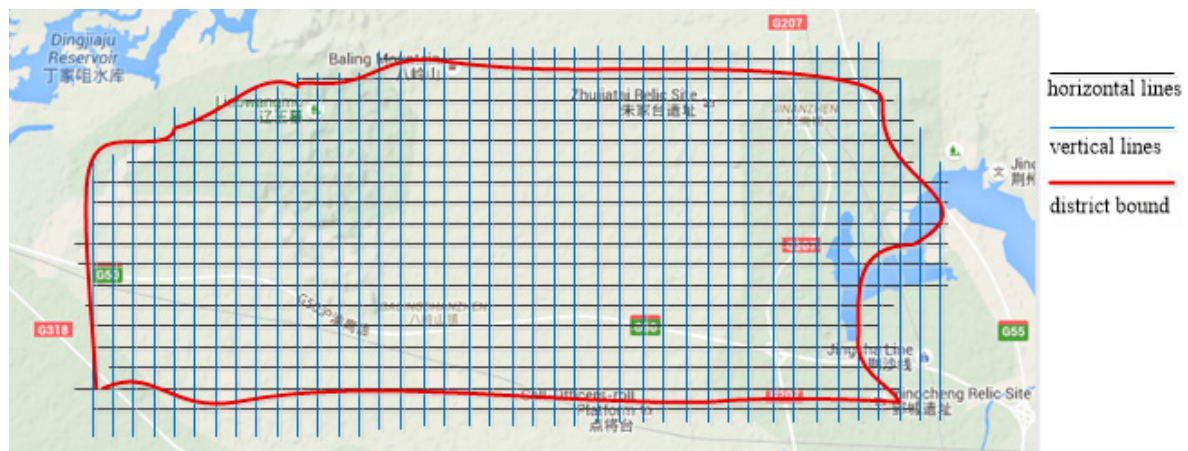**Figure 4.** Framework of the proposed approach.

Figure 5. Light Detection and Ranging (LiDAR) data collection flight grid for obtaining a high-density point cloud.

After obtaining the high-quality point cloud data from the district, filtering and classification processes are implemented to obtain the ground points, as shown in Figure 4. These processing steps are the same as those in traditional DEM production, but the classification step must preserve the archaeological objects to generate an archaeological digital evaluation model (A-DEM), which will be introduced in Section 3.2. Then, an analysis of the ground point pattern of the Chu tombs is presented to construct the archaeological object pattern database, which will be described in detail in Section 3.3. In addition, based on the archaeological object pattern database, the point cloud data are transformed into a feature space, and the tomb remains are extracted from the large-volume LiDAR data, as described in Section 3.4. Finally, exact tombs are identified with LiDAR data and visible remote sensing images, as described in Section 3.5.

3.2. Filtering and Classification to Obtain Ground Points

LiDAR point cloud processing for tomb classification and identification begins with a ground point cloud after the trees, vegetation, and buildings are removed using the popular LiDAR point cloud filtering and classification software Terrasolid. Terrasolid provides both automatic and manual filtering and classification functions [40,41]. For conventional DEM production, all of the objects above the ground should be removed [31,32,42]. The information associated with archaeological remains must be preserved, and the artificial objects under dense trees or vegetation are quite different from other artificial objects, such as buildings and facilities. Thus, the classification with TerraSolid must use different judgments of artificial objects based on their surroundings. This type of processing is manual and based on visible remote sensing images in TerraSolid. Sample point cloud data from the Balingshan district are used to illustrate the process of obtaining the ground points, as shown in Figure 6.
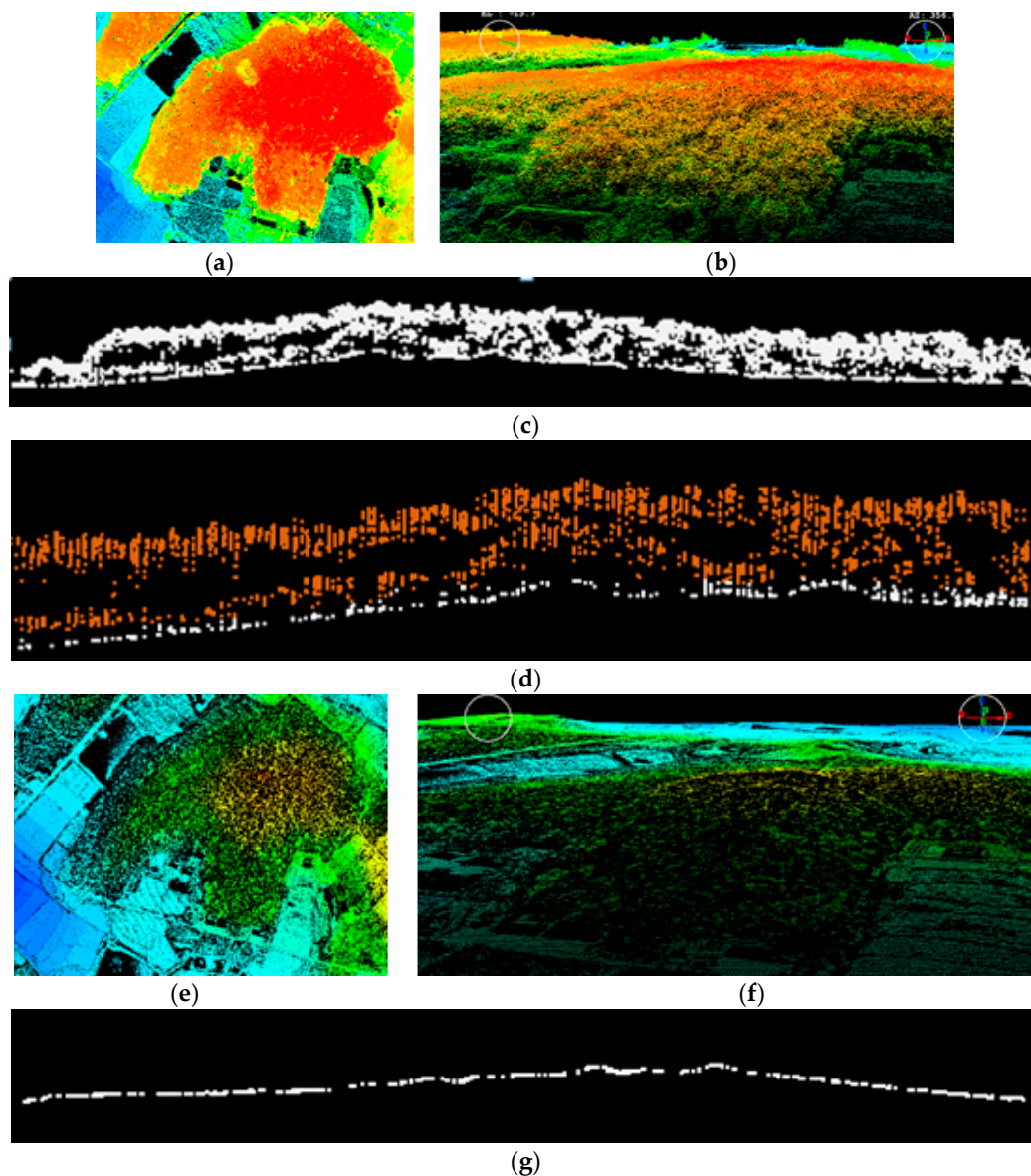

Figure 6. LiDAR point cloud filtering and classification to obtain the ground point cloud. (**a**) Original point cloud; (**b**) 3D view of the original point cloud; (**c**) section of the original point cloud; (**d**) objects in a section of the original point cloud; (**e**) ground point cloud; (**f**) 3D view of the ground point cloud; and (**g**) a section of the ground point cloud.

Figure 6a is the original point cloud. In the 3D view of the original point cloud, all objects are mixed together (Figure 6b). TerraSolid software provides section analysis functions for point cloud filtering and classification (Figure 6c,d). After removing the objects above the ground (Figure 6d), we can classify the ground points (Figure 6e) from the original point cloud dataset. Note that we should combine the visible remote sensing images to assess each object. Additionally, object points under trees and vegetation should be preserved. From the 3D view of the ground points (Figure 6f), trees, vegetation, and buildings are removed from the point cloud, and the cross-section of ground points can be used to assess the classification results (Figure 6g). The final ground points include objects under the trees and vegetation that are different from the ground points used in DEM generation, and they may exclude some data associated with archaeological remains. Using these types of ground points, the A-DEM can be generated for further pattern analysis and to extract and identify tombs.

3.3. Pattern Analysis of Chu Tombs in LiDAR Point Cloud Data

The different archaeological remains from different decades have been affected by different environmental changes, which have different sizes, areas, heights, etc. In this paper, patterns with specific features are proposed to describe different archaeological remains. To obtain the exact patterns of Chu tombs, some known Chu tombs are used for pattern analysis. Specifically, the LiDAR data of the known Chu tombs are used to classify and identify the tomb remains based on the knowledge of archaeologists. The flowchart of pattern analysis is presented in Figure 7.
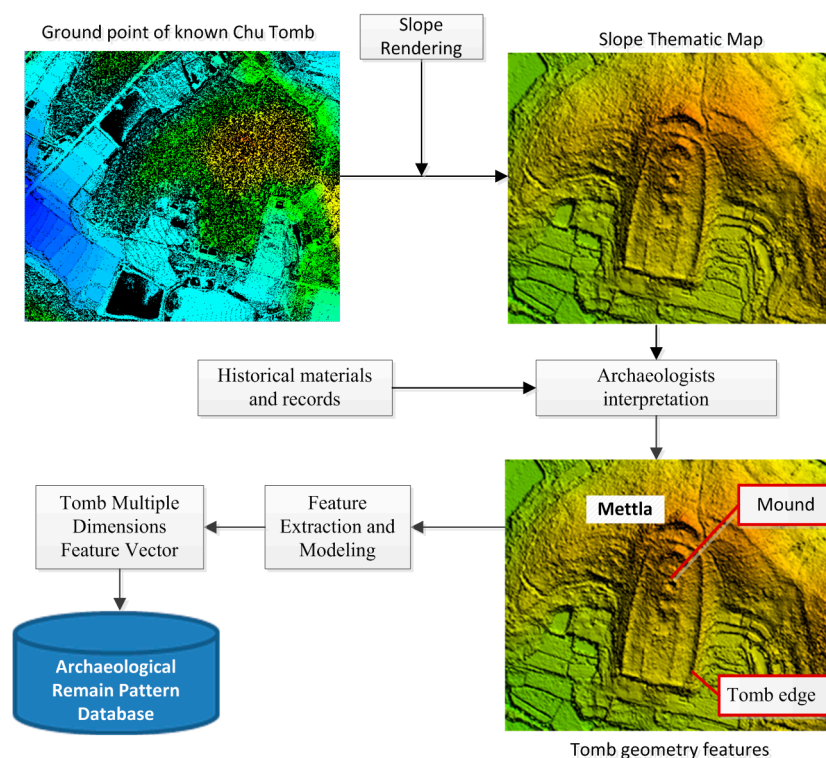

Figure 7. Pattern analysis method used to build a database of the patterns of archaeological remains.

As Figure 7 shows, the LiDAR data associated with some known Chu tombs are used to remove the vegetation and preserve all ground points for pattern analysis. A slope-rendering approach is implemented for the ground point cloud to generate the slope thematic map and obtain visible representations of tomb remains near or in the ground surface. Then, some archaeologists with professional knowledge of the area interpret the tomb remains with the slope thematic map to identify the tomb features, including the mettla, mound, tomb edge, etc., from the terrain. Next, the geometric features of the tomb are calculated and extracted based on the interpretation results.

These features include the height difference, length, width, mettla, and mound size, and they are used to build a multidimensional feature vector of each tomb. All of these feature vectors are added to the archaeological remains pattern database for further processing.

3.4. Feature Transformation and Fuzzy Clustering of Tomb Segments

3.4.1. Feature Transformation

To identify and extract the archaeological remains from the point cloud, feature transformation [30] is performed to enhance the features of archaeological remains. Our proposed approach treats specific spatial parameters as feature factors based on the archaeological remains pattern database, and point cloud data are transferred into a feature domain. The feature factor calculation and feature transformation processes are implemented based on a spatial grid, as described in the following three steps.

Step 1: *Spatial interval selection and grid division*. The spatial grid used for feature transformation must consider the density of the point cloud and the geometric patterns of different archaeological remains. The spatial grid interval *Int* can be calculated using Equation (1):

$$Int = \left\{ iT \,|\, iT < GSD \cap iT < \frac{1}{3} iSize \right\} \tag{1}$$

where *GSD* represents the density of the point cloud, which is the average distance between two LiDAR points, and *iSize* is the minimum geometry required to identify the tomb.

Step 2: *Feature factor calculation*. In this step, the feature value is calculated based on the LiDAR data in each grid, as shown in Equation (2):

$$W_{ij}^k = \alpha \frac{\sqrt{2} \cdot GSD}{D_{ij}^k} + \beta \cdot f_{ij}^k \cdot H_{ij}^k \tag{2}$$

$$f_{ij}^k = \frac{\left(h_{\min}^k - Z_{\min} \right)}{\left(Z_{\max} - h_{\max}^k \right)} \\ H_{ij}^k = h_{\max}^k - h_{\min}^k \tag{3}$$

where *GSD* is the ground spatial resolution of the LiDAR point cloud, which also represents the density of the point cloud; *i* and *j* are the row and column of the grid, respectively; *k* is the number of point clouds in the current grid; H_{ij}^k is the height difference of the current grid; f_{ij}^k is the height scale factor of the current grid; D_{ij}^k is the spatial distance between LiDAR point *k* and the center of the current grid; and α and β are the adjustment parameters used in the feature calculation of each grid.

Step 3: *Feature raster image generation*. In this step, the features of each grid are calculated to convert the massive LiDAR point cloud into feature raster images. With the feature images, archaeological remains extraction and identification can be performed in the raster image domain using traditional image-processing algorithms.

3.4.2. Fuzzy Cluster Algorithm for Tomb Segmentation

Fuzzy clustering is the most popular raster image-processing algorithm for object segmentation [42,43]. In this paper, a fuzzy c-means clustering (*FCM*) algorithm is presented for the tomb segments of the feature raster image.

The cost function of *FCM* is as shown in Equation (4):

$$J(U, c_1, ..., c_c) = \sum_{i=1}^{c} J_i = \sum_{i=1}^{c} \sum_{j}^{n} u_{ij}^m d_{ij}^2 \tag{4}$$

$$\sum_{i=1}^{c} u_{ij} = 1, \forall j = 1, ..., n \tag{5}$$

where u_{ij} is a value between 0 and 1, and the sum of u_{ij} is 1; c_i is the cluster center of fuzzy group *I*; $d_{ij} = \|c_i - x_j\|$ is the Euclidean distance between the centers of fuzzy groups *I* and *J*; and $m \in [1, \infty)$ is a weighted index. A new object function, shown in Equation (6), is constructed to constrain Equation (4) and perform minimization:

$$\begin{aligned} \bar{J}(U, c_1, ..., c_c, \lambda_1, ..., \lambda_n) &= J(U, c_1, ..., c_c) + \sum_{j=1}^{n} \lambda_j \left(\sum_{i=1}^{c} u_{ij} - 1 \right) \\ &= \sum_{i=1}^{c} \sum_{j}^{n} u_{ij}^m d_{ij}^2 + \sum_{j=1}^{n} \lambda_j \left(\sum_{i=1}^{c} u_{ij} - 1 \right) \end{aligned} \tag{6}$$

where $\lambda_j, j = 1, ..., n$, is the Lagrange multiplier of the constraint equation of Equation (4). The conditions required to minimize Equation (6) are given by Equations (7) and (8) based on varying all input parameters.

$$c_i = \sum_{j=1}^{n} u_{ij}^m x_j / \sum_{j=1}^{n} u_{ij}^m \tag{7}$$

$$u_{ij} = 1 / \sum_{k=1}^{c} \left(\frac{d_{ij}}{d_{kj}} \right)^{2/(m-1)} \tag{8}$$

To meet the required conditions of Equations (6)–(8), *FCM* is an iterative process. The cluster center c_i and membership matrix *U* can be determined by the following steps:

(1) *Step 1*: Initialize membership matrix U with a random number based on the constraint of Equation (5).
(2) *Step 2*: Calculate the cluster center ci using Equation (7).
(3) *Step 3*: Calculate the cost function using Equation (4). The iterative process stops when the cost function is less than the given threshold or the change in the cost function is less than the established threshold.
(4) *Step 4*: Recalculate membership matrix *U*; then, go to *Step 2* to run the iterative process.

3.5. Identification and Verification with LiDAR Data and Visible Remote Sensing Images

The Chu tomb detection and identification approach based on the feature raster image includes three stages: feature object segmentation, object identification, and verification, as shown in Figure 8.

With the feature raster image, feature object-based image segmentation is presented to obtain different object sets using the unsupervised *FCM* clustering algorithm, as discussed in Section 3.4.2. Then, object-oriented classification based on the archaeological remains pattern database is performed to identify the tomb objects from the image segmentation object set. The tomb extraction and identification results must be checked and verified with the original point cloud and visible images. Different rendering approaches of the LiDAR point cloud, such as height rendering, slope rendering and local height rendering, are employed to enhance the visualization result for the connection and merging of tomb objects. In addition, visible digital orthophotos are used for the further verification of tombs based on spatial relations and surroundings. Finally, the identified tombs can be located with georeferenced data from both the LiDAR point cloud and the digital orthophotos.
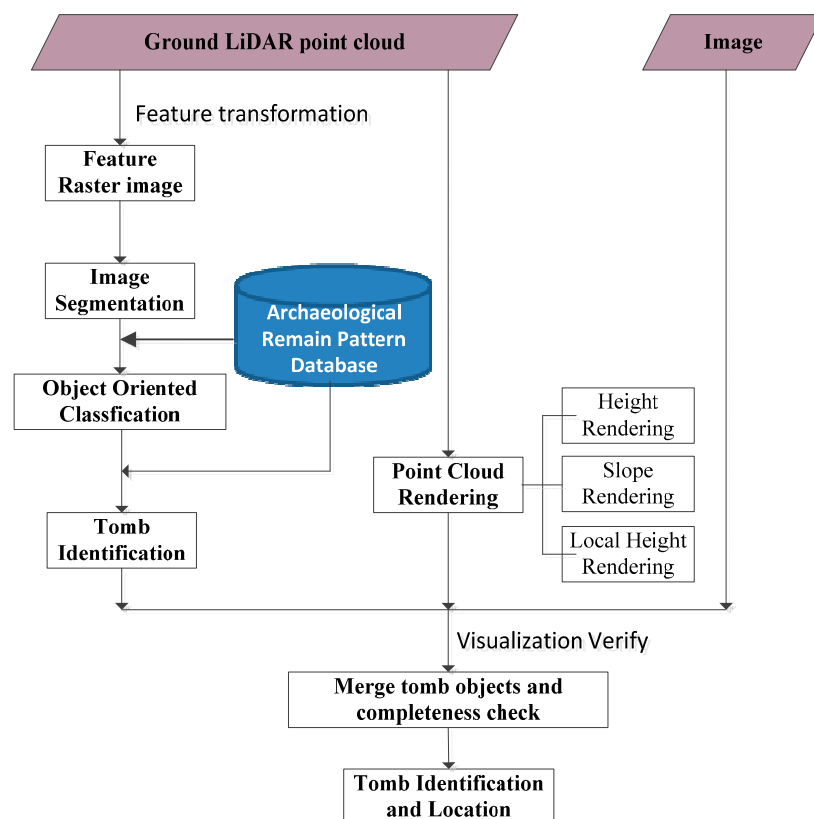
Figure 8. The identification and verification of archeological remains.

4. Results, Analysis and Discussion

With the proposed approach, we adopted a Trimble Harrier 56 Airborne LiDAR System to obtain the LiDAR data from the study area (Figure 1) with a density of more than 16 pts/m^2 in September 2010. The total area was approximately 180 km^2, and the LiDAR data volume was above 1 TB, including the LiDAR point cloud and visible image. All the data were analyzed with the proposed approach together with onsite archaeological exploration. We chose the core region of the Balingshan district, which is approximately 20 km^2, for tomb investigation.

4.1. Chu Tomb Identification Result of the Balingshan District

In the study area, we selected 12 sites with the help of archaeologists to obtain the patterns of Chu tombs. The tombs at the 12 sites cover all types of typical Chu tombs, and have different shapes and sizes. Additionally, the local cultural relics department provided a database of known tombs for verification. We discovered and located 315 tombs with the proposed approach.

In Table 1, the 168 known tombs provided by the local cultural relics department are all included in the list of discovered tombs. Additionally, we identified 147 new tombs, and local archaeologists visited these sites for confirmation.

Table 1. Statistical results of the discovered Chu tombs.

Tomb Patterns Used	Total Number of Discovered Tombs	Number of Known Tombs	Number of New Tombs
12	315	168	147

In Figure 9, three typical regions with high densities of tomb groups are used to illustrate the spatial distribution of Chu tombs. Region 1 and Region 2 were approximately 3 km^2, and Region 3 was less than 1 km^2.
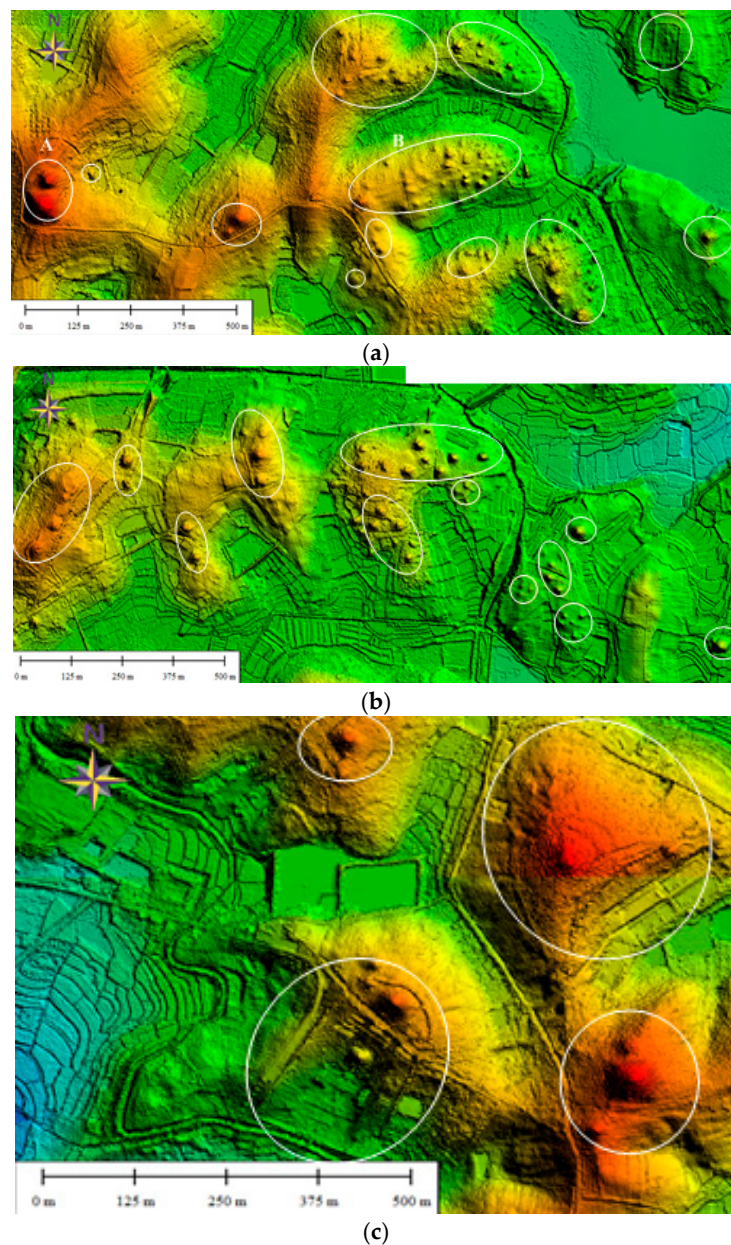
(a)

(b)

(c)

Figure 9. Spatial distribution of Chu tombs in the Balingshan District: (**a**) Chu tombs in Region 1; (**b**) Chu tombs in Region 2; and (**c**) Chu tombs in Region 3.

As Figure 9 shows, the mounds were well exposed in the A-DEM after we removed the vegetation and trees from the LiDAR point cloud. Based on the pattern database of known Chu tombs, we identified and located some unknown Chu tombs. Different types of Chu tombs had different shapes and sizes, which were used to establish tomb specifications and assign grades. In addition, the spatial distribution of Chu tombs was grouped by clan and social class. The A-DEM with archaeological remains is a new geodata product for archaeological research.

Isolated tombs and tomb groups were identified in Region 1. Among the isolated tombs, a large tomb can be seen in the left corner (labeled *A*) of Figure 10c. This tomb had a main mound size of 80 m × 70 m and accompanying mound size of 30 m × 40 m, which indicated that it was a nobility-level tomb. Among the tomb groups, one group exhibited regular alignments (labeled *B*, details in Figure 10b). This tomb group for a clan is called an ancestral hall. Some remains were not actually tombs, but rather sacrificial worship platforms used to offer sacrifices to ancestors, as identified

after on-site investigation. Region 2 had more isolated tombs than Region 1, but the tombs were smaller than those in Region 1. We could not deduce that the levels of tombs in Region 2 were lower than those in Region 1 based on tomb size alone. Notably, the period of tombs is another factor related to the size and level of tombs. The tombs in Region 3 are all isolated tombs that are larger than those in Region 1 and Region 2. One tomb is trapezoidal, with a height of 260 m and a perimeter of 180 m. Another tomb was shaped like an equilateral triangular with a side length of approximately 330 m and a mound height of nearly 20 m. These two isolated tombs could have a level and grade above nobility. Region 3 was known as a Fengjia Tomb, which was a high-level tomb group of Chu nobility. Human activities and economic development are prevalent in this region. A road can be seen that crosses the trapezoidal tomb and goes around the triangular tomb. In 2011, the Archeology Institute of Jingzhou started protective archeological excavations in this region. After approximately two years of detailed investigation, comprehensive exploration, and partial excavations, these tombs were found to be high-level nobility Chu tombs from the Donghan Period (B.C. 770–B.C. 256). In addition, the group may include a certain Chu king's tomb.

4.2. Discovery and Analysis of Four Typical Chu Tombs

We identified approximately 180 km^2 in Jingzhou County where there were potential tombs. Although only 20 km^2 in the Balingshan district was chosen to identify Chu tombs with the proposed approach, we discovered approximately 300 tombs. It was difficult to check and verify each tomb, but our results provide useful georeferenced data for archeological research and preservation. We chose four typical tombs for further analysis with the proposed approach. Figure 10 shows the four typical Chu tombs. Each tomb was assessed with both the A-DEM to reflect the geometry and the visible remote sensing image of the tomb's surroundings.
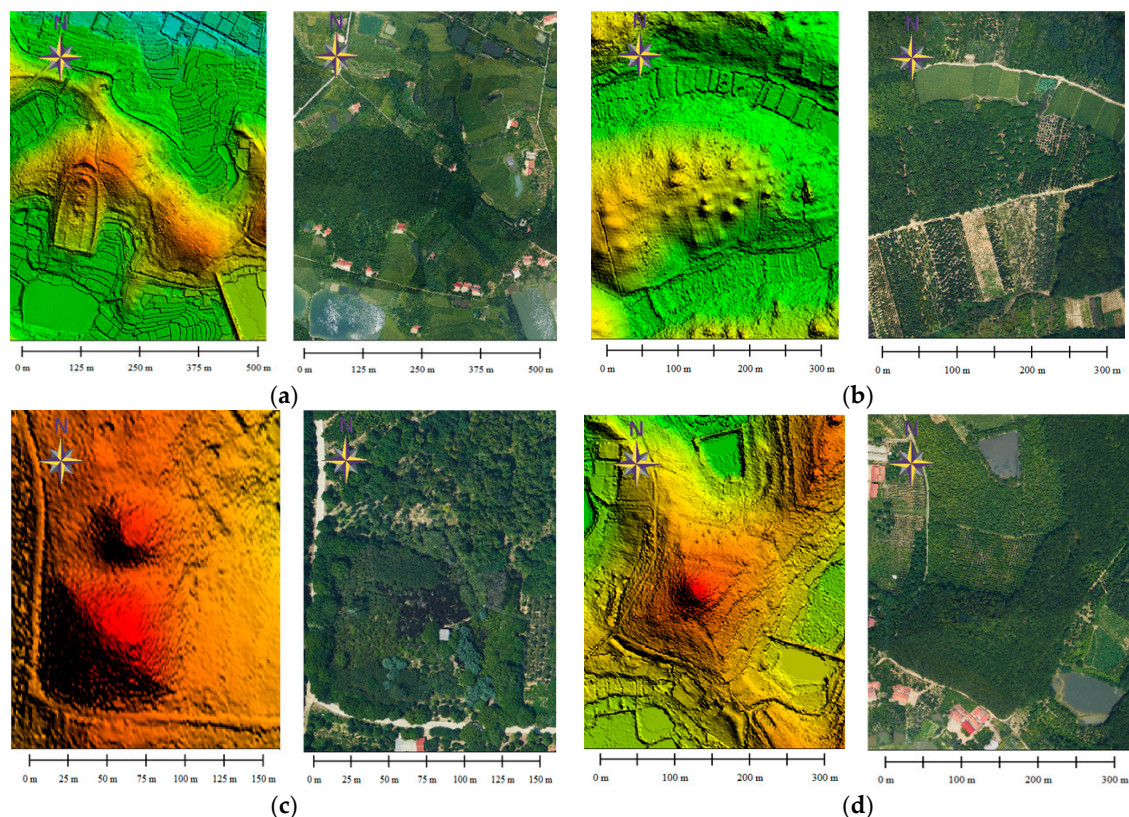

Figure 10. Typical Chu tombs: (**a**) trapezoidal tomb; (**b**) tomb group; (**c**) tomb with two mounds; and (**d**) pyramid mound.

Figure 10a shows another trapezoidal tomb with a height of 260 m and a perimeter of 120 m. This tomb was also an ancestral hall with a well-preserved tomb outline. The main mound is located at the top of the tomb, and the level is clear from bottom to top. Archaeologists call it the 'Moon ancestral hall', and it might be another Chu king's tomb. Figure 10b shows the spatial distribution of the tomb group in Region 1 discussed in Section 4.1. Based on the geometry, shape and structure, it may be a clan tomb for nobility.

Figure 10c shows a high-grade tomb, which might be of certain nobility, as discussed in Section 4.1. These types of tombs were popular Chu tombs. One mound might be a certain funerary tomb, but we are not sure of this designation, and further research is required on this type of tomb. Figure 10d shows a pyramid mound with clear steps. In fact, the archaeologists and local villagers knew there was a tomb here, and they reputed it to be a medium-sized tomb no higher than nobility, called the Lijia Tomb. After studying the A-DEM data, these experts changed their belief and visited the site for further investigation and exploration. The base of the tomb was 170 m × 160 m, with a height of approximately 15 m. Figure 11 shows the 3D view of the Lijia Tomb. Based on the tomb research, A-DEM data and onsite studies, the Lijia Tomb might be a king's tomb, and the king likely had a short reign.
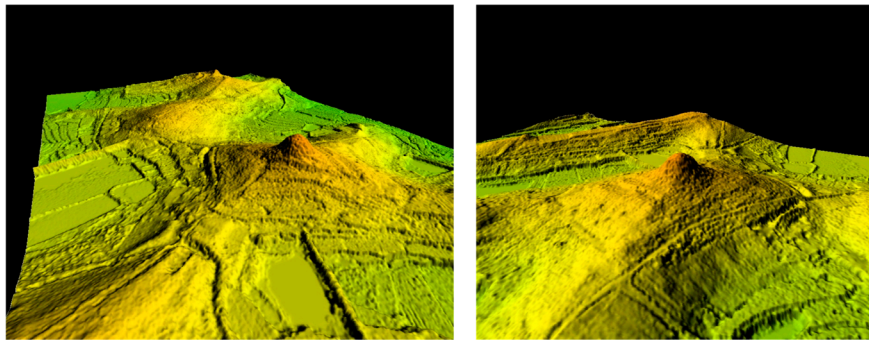

Figure 11. 3D views of the Lijia Tomb.

In addition, we found some tombs that were threatened by human activities and economic development. As we noted in the background section, the Jingzhou district has a high population density, and it was known as a Chu region for more than 2000 years. We do not know exactly how many archaeological sites are in this district. Preservation and research efforts face unpredictable challenges, and archaeologists must continuously perform rescue excavations. The preservation of these archaeological remains is a problem for the local government. With the proposed approach, we discovered that many tombs might have been destroyed by construction, such as road networks, industrial factories, and real estate development. Fortunately, only small parts of these tombs were damaged, and there was no damage to the tomb bodies, as Figure 12 shows.

Although the tomb bodies of these tombs were not destroyed, the threat still exists. The proposed approach provides the possibility of discovering and locating archaeological remains for both local government and archaeologists.
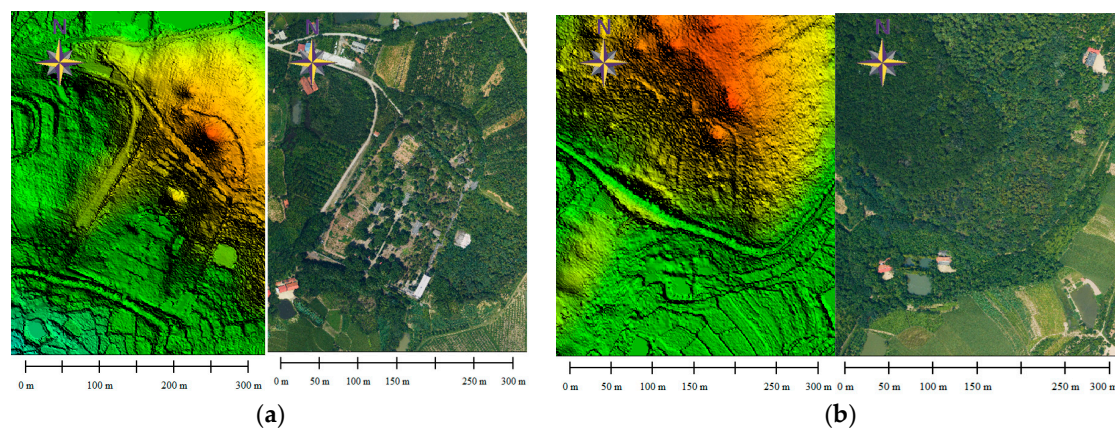
Figure 12. Identification and verification of archaeological remains. (**a**) Road across near the mound; (**b**) Road across the bottom of the tomb.

4.3. Discussion

Technological developments in LiDAR are changing how archaeologists investigate and study the history of archaeological remains under vegetation and even under water in rivers or seas [44]. Microtopographic feature analysis using airborne LiDAR data has been proven to effectively identify Chu tombs in Jingzhou. This method is ideal for tomb investigation and surveying in the historical districts of South China.

However, as in all archaeological prospecting, using microtopographic feature analysis to obtain an A-DEM for tomb identification has inherent methodological and interpretive limitations. The first issue is comparing its classification of the ground points of tombs for historical object preservation with typical ground point classifications. In this case, we focused on the unknown archaeological objects under the vegetation. Artificial objects such as buildings and facilities can be identified based on the surrounding situation. Thus, ground point classification requires manual user assessment with visible remote sensing images. This approach is time consuming, and those performing the point cloud classification must have knowledge of the local archaeology. We only processed 20 km^2 of 180 km^2 in the core region of Balingshan. Although many types of algorithms are available for point cloud classification, the ground point classification required to create an A-DEM poses a continuous challenge due to the different types of tombs in different periods.

Another issue involves the pattern database for tombs. Notably, we knew that most of the tombs in Balingshan were Chu tombs. In addition, we knew the locations and features of some Chu tombs in the district. Thus, we used the LiDAR data from the known Chu tombs to analyze the tomb patterns and support archaeological efforts. The discovered tombs are relatively large tombs, and we are sure there are some archaeological remains that were not identified by the proposed method. Thus, the proposed approach has inherent uncertainty, and we would not repeat the success in other districts without historical records. However, such situations are not common, and archaeological investigation and surveying require interdisciplinary collaboration between remote sensing and archaeology to achieve better results [45]. Moreover, communication with local archaeologists is more important than algorithm optimization.

Issues may be encountered when applying the proposed approach to a wide range of other archaeological remains. One issue is the density of LiDAR point cloud data. We must improve the density of the LiDAR point cloud and obtain more knowledge of archaeological remains in the study area to extract and identify more remains using the algorithm. Although full-wave LiDAR can be used to extract more points under vegetation [5,6], the point density should be determined based on the specific archaeological remains. The associated technology is not the key problem; a lack of historical information and records hinders such studies. Another issue is the efficiency and cost of LiDAR processing for the extraction and identification of archaeological remains.

5. Conclusions

In this study, microtopographic feature analysis was used for tomb discovery and identification in dense vegetation districts using airborne LiDAR data. A new DEM product, A-DEM, was proposed for the detection of archaeological remains. Archaeological features and patterns were interpreted and extracted from the LiDAR point cloud to build an archaeological object pattern database. Based on the patterns of tombs, a fuzzy clustering algorithm considering archaeological object patterns was used for raster feature image segmentation and the detection of archaeological remains. The Chu tombs in the Balingshan district of Jingzhou were used as a case study, and the results show that the proposed approach can identify and extract the different types of Chu tombs from large-volume and massive LiDAR data, including in areas with dense vegetation and trees. These findings can be used by both local governments and archaeologists for archaeological site preservation and research.

Author Contributions: Shaohua Wang and Qingwu Hu conceived the study and wrote the paper; Fengzhu Wang conceived the study; Mingyao Ai performed field data collection and data processing; and Ruofei Zhong implemented the data analysis.

Conflicts of Interest: The authors declare no conflicts of interest.

References

1. Chase, A.F.; Chase, D.Z.; Fisher, C.T.; Leisz, S.J.; Weishampel, J.F. Geospatial revolution and remote sensing LiDAR in Mesoamerican archaeology. *Proc. Natl. Acad. Sci. USA* **2012**, *109*, 12916–12921. [CrossRef] [PubMed]
2. Hritz, C. Contributions of GIS and Satellite-based Remote Sensing to Landscape Archaeology in the Middle East. *J. Archaeol. Res.* **2014**, *22*, 229–276. [CrossRef]
3. Kincey, M.; Batty, L.; Chapman, H.; Gearey, B.; Ainsworth, S.; Challis, K. Assessing the changing condition of industrial archaeological remains on Alston Moor, UK, using multisensor remote sensing. *J. Archaeol. Sci.* **2014**, *45*, 36–51. [CrossRef]
4. Keay, S.J.; Parcak, S.H.; Strutt, K.D. High resolution space and ground-based remote sensing and implications for landscape archaeology: The case from Portus, Italy. *J. Archaeol. Sci.* **2014**, *52*, 277–292. [CrossRef]
5. Lasaponara, R.; Masini, N. Satellite remote sensing in archaeology: Past, present and future perspectives. *J. Archaeol. Sci.* **2011**, *38*, 1995–2002. [CrossRef]
6. Lasaponara, R.; Coluzzi, R.; Masini, N. Flights into the past: Full-waveform airborne laser scanning data for archaeological investigation. *J. Archaeol. Sci.* **2011**, *38*, 2061–2070. [CrossRef]
7. Rączkowski, W. Aerial archaeology. In *Field Archaeology from Around the World*; Springer International Publishing: Cham, Switzerland, 2015; pp. 19–25.
8. Chen, F.; Lasaponara, R.; Masini, N. An overview of satellite synthetic aperture radar remote sensing in archaeology: From site detection to monitoring. *J. Cult. Herit.* **2015**, *23*, 5–11. [CrossRef]
9. Chen, X.T.; Disney, M.I.; Lewis, P.; Armston, J.; Han, J.T.; Li, J.C. Sensitivity of direct canopy gap fraction retrieval from airborne waveform LiDAR to topography and survey characteristics. *Remote Sens. Environ.* **2014**, *143*, 15–25. [CrossRef]
10. Vaughan, M.A.; Young, S.A.; Winker, D.M.; Powell, K.A.; Omar, A.H.; Liu, Z.; Hu, Y.; Hostetler, C.A. Fully automated analysis of space-based LiDAR data: An overview of the CALIPSO retrieval algorithms and data products. In *Remote Sensing*; International Society for Optics and Photonics: Bellingham, WA, USA, 2004; pp. 16–30.
11. Devereux, B.J.; Amable, G.S.; Crow, P.; Cliff, A.D. The potential of airborne LiDAR for detection of archaeological features under woodland canopies. *Antiquity* **2005**, *79*, 648–660. [CrossRef]
12. Bewley, R.H.; Crutchley, S.P.; Shell, C.A. New light on an ancient landscape: LiDAR survey in the Stonehenge World Heritage Site. *Antiquity* **2005**, *79*, 636–647. [CrossRef]
13. Harmon, J.M.; Leone, M.P.; Prince, S.D.; Snyder, M. LiDAR for archaeological landscape analysis: A case study of two eighteenth-century Maryland plantation sites. *Am. Antiq.* **2006**, *71*, 649–670. [CrossRef]

14. Rowlands, A.; Sarris, A. Detection of exposed and subsurface archaeological remains using multi-sensor remote sensing. *J. Archaeol. Sci.* **2007**, *34*, 795–803. [CrossRef]

15. Challis, K. Airborne laser altimetry in alluviated landscapes. *Archaeol. Prospect.* **2006**, *13*, 103–127. [CrossRef]

16. Challis, K.; Forlin, P.; Kincey, M. A generic toolkit for the visualization of archaeological features on airborne LiDAR elevation data. *Archaeol. Prospect.* **2011**, *18*, 279–289. [CrossRef]

17. Doneus, M.; Briese, C.; Fera, M.; Janner, M. Archaeological prospection of forested areas using full-waveform airborne laser scanning. *J. Archaeol. Sci.* **2008**, *35*, 882–893. [CrossRef]

18. Gallagher, J.M.; Josephs, R.L. Using LiDAR to detect cultural resources in a forested environment: An example from Isle Royale National Park, Michigan, USA. *Archaeol. Prospect.* **2008**, *15*, 187–206. [CrossRef]

19. McCoy, M.D.; Ladefoged, T.N. New developments in the use of spatial technology in archaeology. *J. Archaeol. Res.* **2009**, *17*, 263–295. [CrossRef]

20. Masini, N.; Lasaponara, R. Airborne LiDAR in archaeology: Overview and a case study. In Proceedings of the International Conference on Computational Science and Its Applications, Ho Chi Minh City, Vietnam, 24–27 June 2013; pp. 663–676.

21. McCoy, M.D.; Asner, G.P.; Graves, M.W. Airborne LiDAR survey of irrigated agricultural landscapes: An application of the slope contrast method. *J. Archaeol. Sci.* **2011**, *38*, 2141–2154. [CrossRef]

22. Chase, A.F.; Chase, D.Z.; Weishampel, J.F.; Drake, J.B.; Shrestha, R.M.; Slatton, K.C.; Awe, J.J.; Carter, W.E. Airborne LiDAR, archaeology, and the ancient Maya landscape at Caracol, Belize. *J. Archaeol. Sci.* **2011**, *38*, 387–398. [CrossRef]

23. Chase, A.F.; Chase, D.Z.; Weishampel, J.F. Lasers in the Jungle. *Archaeology* **2010**, *63*, 27–29.

24. Rochelo, M.J.; Davenport, C.; Selch, D. Revealing pre-historic Native American Belle Glade earthworks in the Northern Everglades utilizing airborne LiDAR. *J. Archaeol. Sci. Rep.* **2015**, *2*, 624–643. [CrossRef]

25. Johnson, K.M.; Ouimet, W.B. Rediscovering the lost archaeological landscape of southern New England using airborne light detection and ranging (LiDAR). *J. Archaeol. Sci.* **2014**, *43*, 9–20. [CrossRef]

26. Stott, D.; Boyd, D.S.; Beck, A.; Cohn, A.G. Airborne LiDAR for the detection of archaeological vegetation marks using biomass as a proxy. *Remote Sens.* **2015**, *7*, 1594–1618. [CrossRef]

27. Opitz, R.; Nuninger, L. Point Clouds Segmentation of Mixed Scenes with Archeological Standing Remains: A Multi-Criteria and Multi-Scale Iterative Approach. *Int. J. Herit. Dig. Era* **2014**, *3*, 287–304. [CrossRef]

28. Roussel, E.; Toumazet, J.P.; Florez, M.; Vautier, F.; Dousteyssier, B. Using airborne LiDAR in geoarchaeological contexts: Assessment of an automatic tool for the detection and the morphometric analysis of grazing archaeological structures (French Massif Central). In Proceedings of the EGU General Assembly Conference, Vienna, Austria, 27 April–2 May 2014; Volume 16, p. 7160.

29. Fernández-Lozano, J.; Gutiérrez-Alonso, G.; Fernández-Morán, M.Á. Using airborne LiDAR sensing technology and aerial orthoimages to unravel roman water supply systems and gold works in NW Spain (Eria valley, León). *J. Archaeol. Sci.* **2015**, *53*, 356–373. [CrossRef]

30. Kusiak, A. Feature transformation methods in data mining. *IEEE Trans. Electron. Packag. Manuf.* **2001**, *24*, 214–221. [CrossRef]

31. Liu, X. Airborne LiDAR for DEM generation: Some critical issues. *Prog. Phys. Geogr.* **2008**, *32*, 31–49.

32. Mongus, D.; Žalik, B. Parameter-free ground filtering of LiDAR data for automatic DTM generation. *ISPRS J. Photogramm. Remote Sens.* **2012**, *67*, 1–12. [CrossRef]

33. Schindling, J.; Gibbes, C. LiDAR as a tool for archaeological research: A case study. *Archaeol. Anthropol. Sci.* **2014**, *6*, 411–423. [CrossRef]

34. Hare, T.; Masson, M.; Russell, B. High-Density LiDAR Mapping of the Ancient City of Mayapán. *Remote Sens.* **2014**, *6*, 9064–9085. [CrossRef]

35. Mei, J.; Wang, P.; Chen, K.; Wang, L.; Wang, L.; Liu, Y. Archaeometallurgical studies in China: Some recent developments and challenging issues. *J. Archaeol. Sci.* **2015**, *56*, 221–232. [CrossRef]

36. Cook, C.A.; Major, J.S. (Eds.) *Defining Chu: Image and Reality in Ancient China*; University of Hawaii Press: Honolulu, HI, USA, 2004.

37. Bai, X.; Gong, Y.; Yang, H. A potential scavenger of carbon radicals for ancient carbonized silk fabrics: Superoxide Dismutase (SOD). *Herit. Sci.* **2014**, *2*, 27. [CrossRef]

38. Shan, J.; Toth, C.K. (Eds.) *Topographic Laser Ranging and Scanning: Principles and Processing*; CRC Press: Boca Raton, FL, USA, 2008.

39. Lemmens, M. Product Survey on Airborne LiDAR Sensors. *GIM Int.* **2007**, *21*, 24–27.

40. Schuckman, K.; Hoffman, G.R. ARIES: Technology fusion for emergency response. *Photogramm. Eng. Rem. Sens.* **2005**, *71*, 357–360.

41. Terrasolid TerraScan User's Guide. Available online: http://www.terrasolid.com/download/tscan.pdf (accessed on 20 August 2016).

42. Kraus, K.; Pfeifer, N. Advanced DTM generation from LiDAR data. *Int. Arch. Photogramm. Remote Sens. Spat. Inf. Sci.* **2001**, *34*, 23–30.

43. Boskovitz, V.; Guterman, H. An adaptive neuro-fuzzy system for automatic image segmentation and edge detection. *IEEE Trans. Fuzzy Syst.* **2002**, *10*, 247–262. [CrossRef]

44. Harrower, M.J. Hydrology, ideology, and the origins of irrigation in ancient Southwest Arabia. *Curr. Anthropol.* **2008**, *49*, 497–510. [CrossRef]

45. Wiseman, J.R.; El-Baz, F. *Remote Sensing in Archaeology*; Springer Science & Business Media: Berlin, Germany, 2007.